Seedless, Etchless Deposition of Nanocrystalline Diamond Coatings for Performance Improvements of Micro End Mills using Carbon Ion Implantation

ICOMM 2011 No.139

Christopher D. Torres[1], Patrick J. Heaney[2], Kumar Sridharan[3], Guoping Cao[4], Anirudha V. Sumant[5], Robert W. Carpick[6], and Frank E. Pfefferkorn[7,*]

[1]Christopher D. Torres; Mechanical Engr., University of Wisconsin-Madison, USA; e-mail: cdtorres@wisc.edu
[2]Patrick J. Heaney; NCD Technologies, LLC, Madison, WI, USA; e-mail: patrick@ncdtechnologies.com
[3]Kumar Sridharan; Engr. Physics, University of Wisconsin-Madison, USA; e-mail: kumar@engr.wisc.edu
[4]Guoping Cao; Engr. Physics, University of Wisconsin-Madison, USA; e-mail: gcao@wisc.edu
[5]Anirudha V. Sumant; Center for Nanoscale Materials, Argonne National Laboratory, USA; e-mail: sumant@anl.gov
[6]Robert W. Carpick; Mechanical Eng. & Applied Mechanics, University of Pennsylvania, USA; e-mail: carpick@seas.upenn.edu
[7]Frank E. Pfefferkorn; Mechanical Engr., University of Wisconsin-Madison, USA; e-mail: pfefferk@engr.wisc.edu*

INTRODUCTION

Tungsten carbide (WC) with a cobalt binder is the typical tooling material used for micro cutters. However, its stiffness limits its use when machining certain materials, especially adherent materials such as Al. The application of nanocrystalline diamond (NCD) coatings has been shown to dramatically improve WC micro tool performance machining Al, eliminating adhesion, lowering the cutting forces, and improving workpiece finish [1]. Approximately 4-8% Co content, found on the surface of the WC grains, is typically used to improve tool ductility and toughness [2]. The presence of this Co is detrimental to the diamond deposition process, by limiting the adhesion of the diamond film or preventing the synthesis of the diamond film altogether [3-4]. A common solution is the removal of surface Co using an acid etching process. However, this treatment will result in embrittlement of the cutting edges and premature cutting edge fracture [2, 5].

To prevent tool embrittlement, and produce a surface that leads to well-nucleated, adherent diamond films, carbon ion implantation (CII) was performed on the as-received tool surface using plasma source ion implantation (PSII) without acid etching. PSII is a non-line-of-sight technique for surface modification of materials [6]. The carbon ions serve multiple beneficial purposes. First, they create nucleation sites for the initial diamond deposition on the tool, thereby eliminating the need to seed the surface with diamond nanoparticles. Secondly, they lead to the formation of a thin layer of cobalt carbide that passivates the surface cobalt and prevents the diffusion of Co to the surface at elevated temperatures during diamond deposition, thus preventing the detrimental interaction of Co with the depositing diamond film [7-8]. In many brittle materials, ion implanted surfaces exhibited higher hardness and wear-resistance. This is caused by induced compressive stresses in the near-surface regions from the implantation process, which inhibit crack nucleation [9]. Finally, the shallow depth and compositionally-graded nature of the modification caused by the CII creates a thin transition layer between the bulk WC and the diamond coating, and does not result in a brittle WC layer.

This study compares the cutting performance of (1) as-received uncoated, (2) acid etched plus seeded plus nanocrystalline diamond (NCD) coated, (3) carbon ion implanted (CII) plus NCD coated, and (4) only CII micro end mills.

EXPERIMENTAL PROCEDURE

Commercially available, 300 µm diameter, 2-flute end mills (PMT part TS-2-0120-S) were used throughout the machining tests. The end mills were tested by dry slot milling 6061-T6 aluminum. Milling parameters were held constant throughout the study to determine the overall effect of the surface preparation used before diamond deposition. For comparison, tools to be coated were subjected to either a hydrofluoric acid etch for approximately 4 seconds or to CII at a pulse voltage of 25 kV for approximately 1 hour in order to passivate the surface Co. Tools were then placed in a hot-filament chemical vapor deposition (HF-CVD) chamber for diamond deposition. Changes in tool condition, cutting forces, and milled surface finished were compared between uncoated, standard (etched and seeded) diamond coated, and CII and diamond coated end mills after cutting a 250 mm length of slots.

Due to the small surface area of the cutting section of the micro end mills, commercially available, uncoated, grade C-2 WC cutting inserts were used for surface characterization. The inserts were prepared in exactly the same manner as the end mills.

A. CARBON ION IMPLANTATION

For the carbon ion implanted samples, the tools were first cleaned using a two steps process: by ultrasonication in ace-

* corresponding author

tone, and then in methanol. After cleaning, the WC end mills had their shanks coated with silver paste (to increase electrical conduction) and placed within an aluminum block with approximately 3 mm of the tool exposed to the implantation plasma. This was done to prevent arching from occurring during the implantation caused by the combination of the small tool volume and high electron densities. A diagram of the plasma chamber is shown in Figure 1. The tools were first subjected to a sputter clean operation within the implantation chamber using argon (Ar) and then followed by the carbon ion implantation procedure. The nominal process parameters are listed in Table 1. The process and conditions are similar to those in Nono *et.al*. [7] and Walter *et.al*. [10].

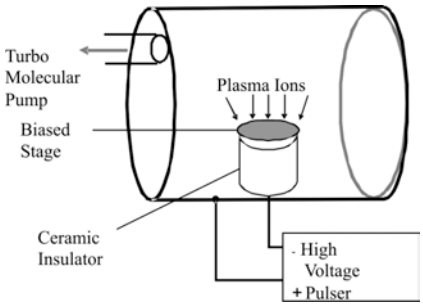

Figure 1. Carbon ion implantation chamber.

For sputter cleaning, the chamber was pumped down to 10^{-7} Torr. The chamber was back-filled to ~15 mTorr using Ar gas. A glow discharge system was used to create an Ar plasma. A bias voltage of -5 kV was applied to the inserts for 10 minutes for sputter cleaning. The process was then turned off and the chamber pumped back to 10^{-7} Torr.

For carbon ion implantation, the chamber was then back-filled to 0.8 mTorr with CH_4 gas. Hot filaments were used to create a plasma of hydrocarbon ions and electrons. The tools and stage were then pulsed at -20 kV for a total of 1 hour, resulting in a total retained dose of about 3 x 10^{17} ions/cm^2.

Table 1: Nominal conditions for Ar sputtering and carbon ion implantation

	Ar Sputter Cleaning	Carbon Ion Implantation
Pressure (mTorr)	30	0.8
Energy (kV)	5	20
Plasma Creation	Glow Discharge	Hot-Filament
Precursor Gas	Ar	CH_4
Dose (ions/cm^2)	n/a	3 x 10^{17}
Process Duration (min)	10	60

B. CHEMICAL ETCHING

The etched tools were prepared by etching in a hydrofluoric (HF) acid solution for 4 seconds. The solution consisted 10 ml HF, 20 ml nitric acid, and 30 ml of de-ionized water. After 4 seconds the micro end mills were removed from the solution and rinsed with DI water. Previous analysis using XPS has shown that 7 seconds of etching was required to remove Co from the surface. However, experimental testing of the micro end mills had determined that optimal coating and tool life was achieved using 4 seconds of etching.

C. DIAMOND GROWTH

The etched WC tools were then seeded by ultrasonication with an ultra-dispersed diamond (UDD) [nanoparticles] in dimethyl sulfoxide (DMSO) and methanol solution for 15 minutes. The samples were then unltrasonicated in pure methanol for 10 minutes as a rinsing step. The tools were dried in a stream of nitrogen gas.

The carbon ion implanted tools received no further surface preparation (i.e., no etching, no cleaning, no seeding) and went directly from the PSII chamber to the HF-CVD chamber.

The samples were individually loaded into our HF-CVD chamber, which was then evacuated to a base pressure of 0.10 Torr. Diamond synthesis was performed using a gas chemistry of 4% methane and 96% hydrogen controlled by flow rate at a pressure of 30 Torr. The gas mixture was flowed over tungsten filaments (at 2000 °C) which dissociated the gasses into carbon radicals and atomic hydrogen. The radicals react with the surface, either diamond seeds (etch and seed) or carbides (CII), to create diamond. Both the filament and substrate temperatures were monitored closely to maintain consistent growth conditions between samples. A more complete description of the growth process can be found in Heaney *et.al*. [11].

The growth times were varied from 2 to 5 minutes for each type of surface preparation to determine the minimum growth time required for diamond grains to coalesce into a continuous NCD coating.

D. SURFACE CHARACTERIZATION

The diamond surface morphology was observed by scanning electron microscopy (SEM) (Leo 1530). The chemical content was monitored on the WC inserts by X-ray photoelectron spectroscopy (Perkin–Elmer PHI 5400 ESCA) employing monochromatized Al Kα radiation at 300 W and 20 mA. WC inserts were depth profiled before and after deposition to monitor compositional changes. Raman spectroscopy (Horiba Jobin Yvon LabRam ARAMIS) was used as a method to determine diamond film quality. This particular system allowed for direct Raman measurement on the micro end mills using a 532 nm YAG laser.

E. MACHINING TESTS

Figure 2 illustrates the test setup used for the machining experiments. A high-speed spindle (NSK-HES500) with electric drive and ceramic bearings was mounted to the spindle of a CNC milling machine (HAAS TM-1). A runout of 1 µm was measured on the tool shank during low-speed manual rotation of the spindle. A constant spindle speed of 40,000 rpm and feed rate of 250 mm/min were used to dry mill full-width slots in 6061-T6 aluminum for all of the experiments (Table 2).

The tests consisted of machining a single full-width channel 50 mm long and 45 μm deep, in a 50 mm × 50 mm × 4.8 mm 6061-T6 aluminum block under dry conditions. The workpiece was mounted on a piezo-electric force dynamometer (Kistler 9256C2) before its surface was prepared by facing with a half inch end mill to ensure flatness within 3 μm. Each tool was fixed in the high speed spindle and then aligned to the workpiece using an optical magnification system. The alignment uncertainty was ± 5 μm in the z-axis.

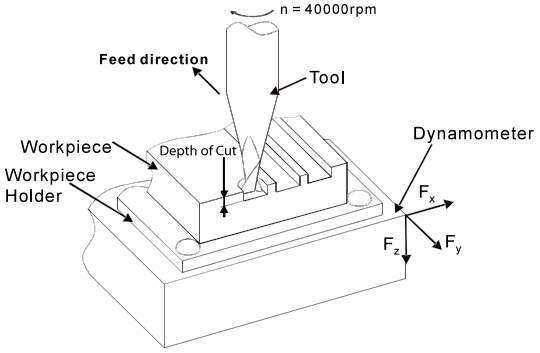

(a)

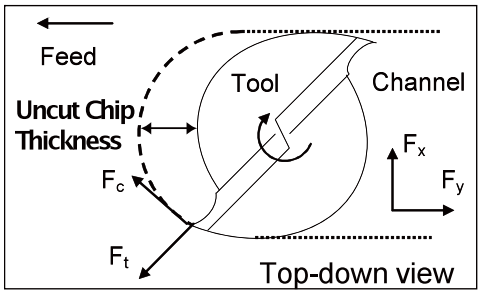

(b)

Figure 2. Schematic of micro end milling: (a) 3D view of experimental setup, (b) end view of the cutting process.

Table 2: Milling parameters

Workpiece Material	6061-T6 Aluminum
Temperature / R.H.	~23°C / ~85%
Tool (end mill):	PMT Model TS-2-0120-S
Material	0.4 μm grain WC-Co
Diameter	305 μm (0.012 in.)
Flutes	2
Helix	30º
Coating	300-450 nm NCD **or** None (bare WC)
Spindle Speed	40,000 rpm
Feed	250 mm/min
Chip Load	3.125 μm
Depth of Cut	45 ± 5 μm
Width of Cut	300 ± 2 μm

The end mills and the milled channels were inspected after 250 mm of linear travel (i.e., after cutting five slots). SEM was used to determine tool and cutting edge condition before and after milling. Milled channels were analyzed using white light interferometry (Zygo NewView 6400).

RESULTS

A. XPS DEPTH PROFILING OF CII SURFACE

XPS depth profiling was done on the WC inserts before and after implantation. The depth profile was recorded in seconds of sputter time. The sputter rate was calculated by sputtering 3 different spots on a sample insert and then measuring the depth with white light interferometry. These three spots were then averaged to calculate the sputter rate of 3 nm/minute. The error in this calculation was ±0.5 nm which could yield a large difference in the depth profile information.

Before implantation the depth profile showed no difference in concentration through the bulk of the insert (Figure 3 a). There was a slight change in atomic concentration between the first and second scans, before sputtering, suggesting that there was a thin layer of water vapor which would be expected since the sample was exposed to ambient conditions.

Figure 3 (b) is an XPS depth profile of a carbon ion implanted WC insert. This profile shows high carbon content with suppressed tungsten and cobalt content at the surface. As the depth of the profile increases, the carbon content decreases while the cobalt and tungsten content increase until the concentrations of the three elements return to the bulk concentration. The largest change in concentration occurs up to a depth of 5 nm, with an additional sputter depth of 10-20 nm required for the concentration to return to the bulk average. The cobalt percentage stabilizes after a depth of 10 nm, while the carbon and tungsten concentrations stabilized after 20 nm.

There are a number of challenges in collecting accurate, quantitative XPS spectra with these samples. The first challenge is that the samples are relatively rough (100-200 nm RMS), the chamber does not have a rotation stage, and the sputter gun is angled from the surface normal. Together, these factors result in sputtering shadows, creating uneven sputtering rates throughout the sample, but still sampled in the spectra. This could account for the higher than expected oxygen levels. A source of error in the atomic percentages is that the values can be artificially inflated because the XPS software requires that the content add up to 100%. The final source of error is the fact that the tungsten and cobalt percentages are determined from peaks from the 4th valence band, requiring a large scaling factor to compare to the oxygen and carbon peaks from the 1st valence band.

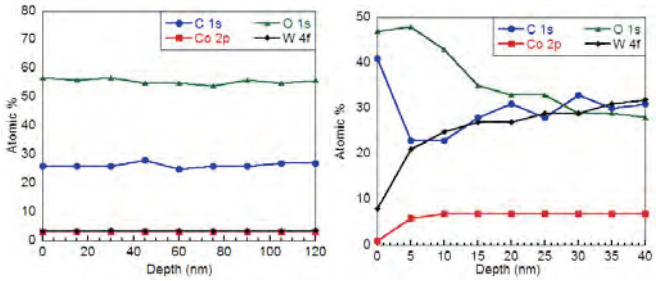

(a) (b)

Figure 3. XPS depth profile of atomic percent of an (Left) as received WC insert and (Right) of a CII WC insert.

A Raman spectrum for an NCD coating grown on a carbon ion implanted micro end mill is shown in Figure 4. The CII-NCD film possessed a sharp peak around 1332 cm^{-1}, which is indicative of sp^3-bonded carbon [12-13]. In addition, the spectra contain a large hump around 1580 cm^{-1} caused by the presence of amorphous and graphitic sp^2-bonded carbon [12-13], which is largely found at the grain boundaries of the diamond films [14]. From the Raman spectra, it was clear that the diamond films are of high quality containing a significant fraction of sp^3-bonded carbon.

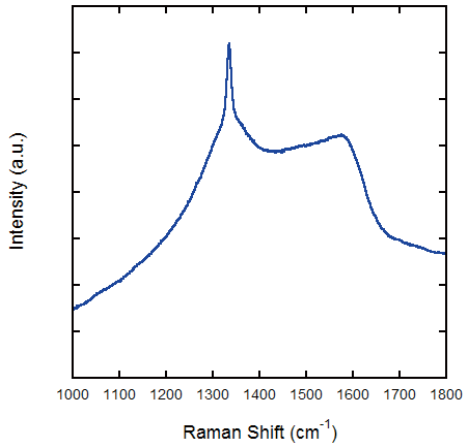

Figure 4. Raman spectrograph of the CII-NCD diamond coating.

B. DIAMOND GROWTH AND TOOL CONDITION BEFORE MILLING

Figure 5 compares the cutting edges of uncoated, etched plus NCD coated, and CII plus NCD coated end mills. Figure 5(c) shows that the CII implanted tools are able to produce a well nucleated, completely coalesced NCD coating without any indication of detrimental growth caused by the tool's cobalt content or the absence of the nanodiamond seeding step. Comparing cutting edge radii, the thin NCD coatings does not significantly blunt the micro end mills and results in a cutting edge radius between 1.1-1.5 µm (Figure 5b,c). Conversely, as-received micro end mills have a cutting edge radius ranging between 0.75 - 1 µm (Figure 5a).

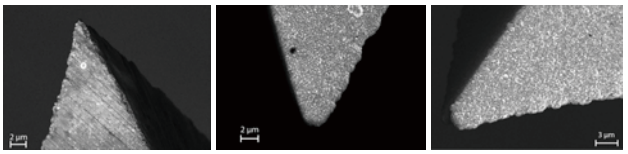

(a) (b) (c)

Figure 5. SEM images of new end mills' cutting edges: (a) uncoated, (b) etched + seeded + NCD coated, (c) CII + NCD coated.

C. TOOL CONDITION AFTER MILLING

The tool condition after an uncoated tool milled 250 mm is shown in Figure 6a,b. Cutting edge fracture is the main mode of tool deterioration, and is followed by abrasive wear.

For the acid etched plus NCD coated end mills, large-scale cutting edge failure is evident in Figure 6c,d. This suggests embrittlement of the cutting edge caused by the removal of cobalt, resulting in significant coating delamination and blunting of the cutting edge. This behavior occurs frequently, although the etched plus NCD coated tools do show major performance improvements over uncoated tools overall, as previously reported [1].

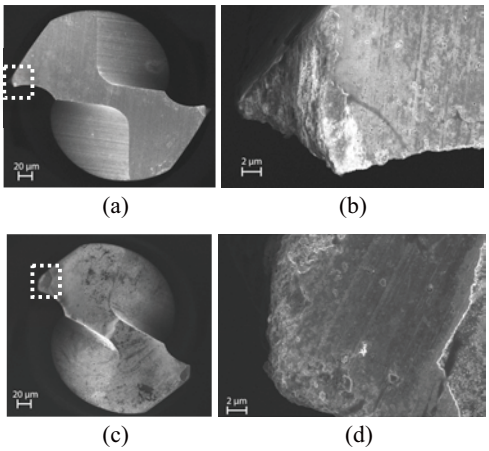

(a) (b)

(c) (d)

Figure 6. SEM images of tools after 250 mm of milling: (a) uncoated , (b) cutting edge and (c) acid etched + NCD coated , (d) cutting edge.

Unlike the uncoated and etched plus NCD coated end mills, the CII plus NCD coated end mills do not show any indication of cutting edge fracture (Figure 7). In fact, one of the cutting edges remained completely intact (Figure 7b). While coating delamination did occur on the other cutting edge (Figure 7c), there was no indication of severe edge fracture. The observable abrasive wear (Figure 7c) on this edge suggests that the delamination event occurred early in the cutting process. The results indicate that the CII did not negatively affect the structural integrity of the cutting edge, instead it may have enhanced the integrity. This could be the result of ion implantation introducing compressive stresses to the surface. This inhibits the nucleation and propagation of microcracks that lead to fracture [9].

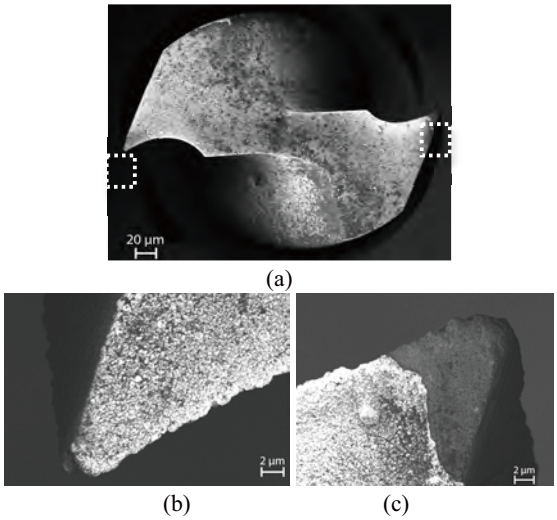

(a) (b) (c)

Figure 7. SEM images of CII + NCD coated end mill after 250 mm of linear milling: (a) end mill, (b) left and (c) right cutting edges.

Figure 8 compares the average change in both cutting edge radius and tool diameter after 250 mm of milling. The etched plus seeded plus NCD coated end mills experienced the most drastic change in both the tool diameter and cutting edge radius. This is largely caused by the removal of cobalt from the tool, causing significant brittle fracture to occur on the cutting edges. It is now believed that the embrittlement of the tool initiates edge fracture, which takes the coating with it, thereby initiating coating delamination. Uncoated end mills also experienced a significant change in average tool diameter and cutting edge radius, but the presence of surface cobalt prevents fracture from occurring at the same scale as observed for the etched plus seeded plus NCD coated end mills. The CII plus NCD coated tool shows the least amount of average change in both the tool diameter and cutting edge radius, even after the delamination of one of the cutting edges (Figure 7c). This indicates that CII is able to produce a well adherent NCD coating without embrittlement of the cutting tool. The tools are able to maintain a rather sharp cutting edge even after coating delamination has occurred.

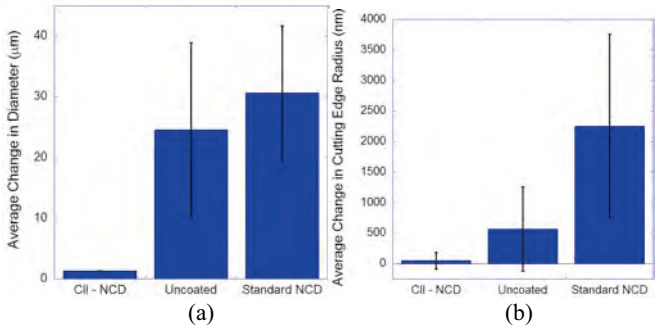

(a) (b)

Figure 8.Comparison of 300 µm diameter tools after 250 mm of milling: (a) average change in tool diameter, and (b) average change in cutting edge radius.

To further verify the wear benefit associated with the CII-NCD coated tools, additional machining tests were performed with end mills that had only been carbon ion implanted. Images of these tools after 250 mm of milling are shown in Figure 9. Much like the CII-NCD coated end mill, one of the cutting edges did not show an indication of cutting edge fracture, only abrasive wear. By comparison, significant fracture of all cutting edges was experienced by all the uncoated end mills within the first 100 mm of milling (Figure 6). However, one of the cutting edges on the tool did experience cutting edge fracture (Figure 9b). This failure, along with the delamination experienced by the CII-NCD end mill, may be attributed to the lack of tool rotational symmetry. The asymmetry results in a non-uniform cutting process across the cutting edges, with one cutting edge removing more material than the other. This increase in load will result in premature edge wear (abrasion and fracture) until a stable tool geometry is produced.

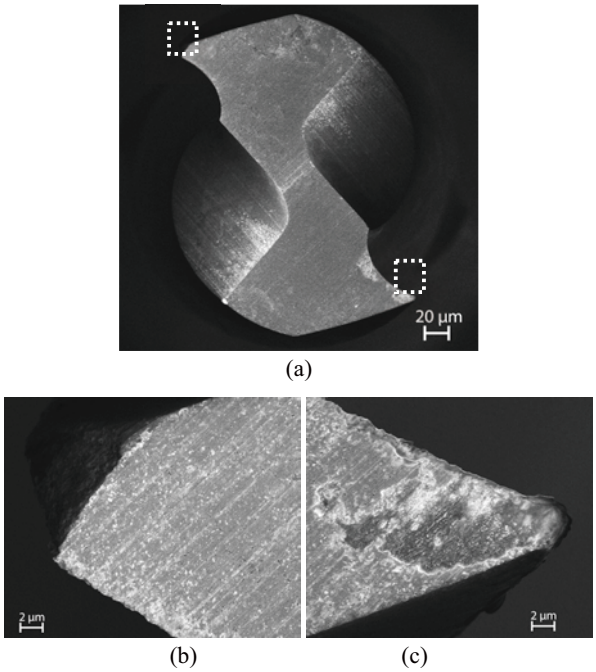

(a) (b) (c)

Figure 9. SEM micrograph of CII + NCD coated: (a) tool, (b) left, and (c) right cutting edges after 250 mm of linear milling.

D. CHANNEL AND SURFACE FINISH COMPARISON

Images of the cut channels after 250 mm of milling are depicted in Figure 10. The uncoated tool produced a significant amount of burring during milling, largely caused by the drastic increase in cutting edge radius. This increase shifts the mode of material removal from a chip formation mechanism to a ploughing mechanism. As expected with large-scale edge failure, burring was evident with the etched and NCD coated end mill. However, the magnitude of burring was noticeably reduced compared to that produced by uncoated tools. This indicates that even after extensive delamination, the NCD-coated tool is still able to provide improved machinability. This improvement is attributed to the presence of the NCD coating still within the flutes of the end mills. This prevents adhesion of the chips to the tool surface during evacuation, resulting in lower cutting forces and a

cleaner surface finish as the cut chips have a clear exit path from the cutting zone.

Even with the sharper cutting edge radius, the tools that are only treated with CII (not coated) produced a significant amount of burring. This is caused by a large amount of the aluminum workpiece material adhering to the tool cutting edges and flutes, resulting in a significant built up edge and difficulty in evacuating cut chips. Because of the clogged flutes and larger effective cutting edge, a large fraction of the workpiece material will plastically flow underneath the cutting edge, forming burrs.

The CII-NCD coated end mills produced burr-free channels after 250 mm of linear cutting distance, demonstrating significantly improved performance. Again, this is caused by the decreased adhesion and friction between the NCD coating and workpiece, allowing the chips to easily move up the tool's flutes from the cutting zone and prevent the formation of a built up edge.

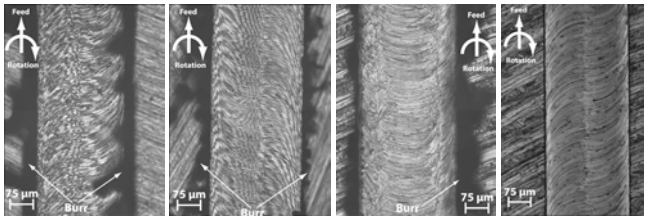

(a) (b) (c) (d)

Figure 10. Optical images of channels milled by: (a) uncoated, (b) etched and NCD coated, (c) CII, (d) CII-NCD coated end mill.

E. CUTTING FORCES

Analysis of the cutting forces during testing confirmed many of the observations from the images of the micro end mills and milled channels. Average measured maximum cutting and thrust forces for each tool are shown in Figure 11 at five different cutting distances.

In general, the uncoated tool experienced higher cutting forces throughout the test. The large force spike around 100 mm of milling distance is associated with significant cutting edge failure, resulting in an effective negative rake angle. Note that a chip load of 3.125 µm was used for all tests (Table 2). The negative rake angle results in larger thrust (i.e., radial) forces that promotes side flow of material, hence burr formation. After tip fracture, the main mode of tool wear shifts towards abrasive wear along the flank face of the cutting edge. This results in sharpening of the cutting edges and a subsequent reduction of cutting forces. The cutting edges then stabilize into a larger radius (~1.75 µm), effective positive rake angle tool with a minimal amount of abrasive wear occurring along the tool's flank face.

For the etched plus NCD coated end mills, significant fracture is again depicted by an increase in cutting forces around 100 mm of milling. As evident with the milled channels, there is still a performance benefit associated with the NCD coating, even after severe cutting failure and coating delamination, with the milling forces not increasing as drastically as the uncoated tool. However, due to the embrittlement of the cutting edges caused by the removal of surface cobalt, the cutting edges will experience several iterations of fracture and subsequent sharpening before a rigid, stable tool geometry is obtained. This results in several drastic increases in the milling forces, along with a larger overall cutting edge radius (~5.5 µm).

The increase in fracture and wear resistivity generated by the carbon ion implantation results in more consistent cutting forces throughout all the experimental cuts (both CII and CII plus NCD tools). The bare and the NCD coated ion implanted end mills experience a spike in cutting forces within the first 50 mm of milling which corresponds to the initial break-in of the tool into a more symmetrical tool shape. After the initial fracture, there is a drop in the cutting forces indicative of the sharpening of the cutting edge due to excessive abrasive wear on the negative tool angle. Once the tools have worn into a stable cutting geometry, there is a substantial drop in wear, resulting in stable cutting forces throughout the rest of the test. The lower thrust forces are indicative of the cutting edges remaining relatively sharp throughout the experimental cuts. The higher cutting force experienced by the bare CII end mills indicates an excessive amount of workpiece material adhering within the flutes. The higher cutting forces are required to overcome the workpiece adhesion and push the cut chips up the flutes. As expected, the NCD coating further decreases the cutting forces by preventing adhesion of the workpiece material to the tool's surface.

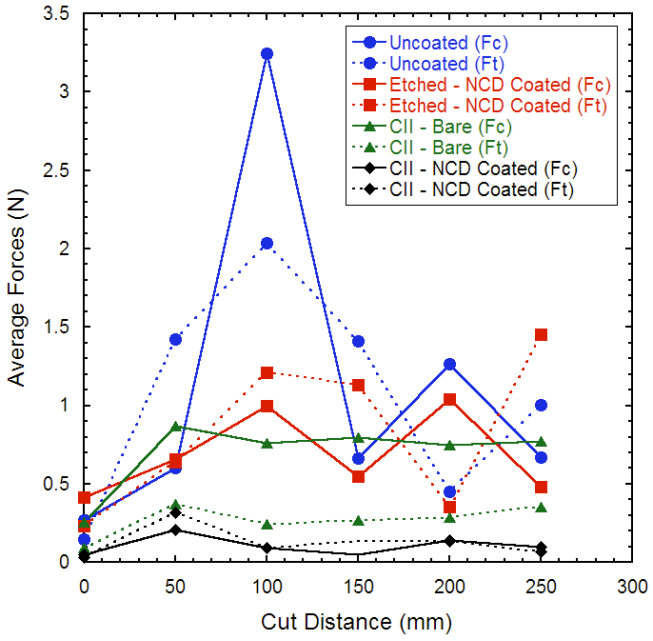

Figure 11. Average cutting and thrust forces for uncoated, standard NCD coated, CII only, and CII-NCD coated end mills at 5 different cut distances.

CONCLUSIONS

Carbon ion implantation (CII) is able to produce a high diamond nucleating density for NCD film growth on tungsten carbide with 6-8% cobalt (WC-Co) tool surface, without the necessity of a diamond seeding step. CII also

passivates the Co phase which is known to have a detrimental effect on diamond film growth. Unlike acid etching, CII does not negatively affect the structural integrity of the tool's cutting edges. In fact, observations suggest that it improves both the fracture and wear resistance of the cutting edges as compared to an as-received uncoated tool. This results in an improvement in NCD coating adhesion and tooling capable of longer, burr-free milling without significant cutting edge failure.

ACKNOWLEDGEMENTS

Support of this work by NSF Grants CMII-0700794 / 0700351, NSF supported shared facilities and the Innovation & Economic Development Research Program at the University of Wisconsin-Madison is gratefully acknowledged. Use of the Center for Nanoscale Materials at Argonne National Laboratory was supported by the U. S. Department of Energy, Office of Basic Energy Sciences, under Contract No. DE-AC02-06CH11357. The authors would like to thank David Burton from Performance Micro Tool for supplying micro end mills.

NOMENCLATURE

CII-NCD	Tool that is carbon ion implanted followed directly by NCD coating.
CII + NCD	
CII plus NCD	
Etched + NCD	Tool that is acid etched, seeded, and then coated with NCD.
Etched + seeded + NCD	
Standard NCD	
NCD	Nanocrystalline diamond.
Uncoated	As-received WC-Co tool without any treatment.

REFERENCES

[1] C. D. Torres, P. J. Heaney, A. V. Sumant, M. A. Hamilton, R. W. Carpick, and F. E. Pfefferkorn, "Analyzing the performance of diamond-coated micro end mills," *International Journal of Machine Tools and Manufacture,* vol. 49, no. 7-8, 2009, pp. 599-612.

[2] J. A. E. Johnson, *Mechanical properties at room temperature of four cermets of tungsten carbide with cobalt binder*, National Advisory Committee for Aeronautics, Washington, DC, United States, 1954.

[3] A. K. Mehlmann, A. Fayer, S. F. Dirnfeld, Y. Avigal, R. Porath, and A. Kochman, "Nucleation and growth of diamond on cemented carbides by hot-filament chemical vapor deposition," *Diamond and Related Materials,* vol. 2, no. Compendex, 1993, pp. 317-322.

[4] B. S. Park, Y. J. Baik, K. R. Lee, K. Y. Eun, and D. H. Kim, "Behaviour of Co binder phase during diamond deposition on WC-Co substrate," *Diamond and Related Materials,* vol. 2, no. 5-7 pt 2, 1993, pp. 910-917.

[5] M. J. Jackson, M. D. H. Gill, H. Sein, and W. Ahmed, "Manufacture of diamond-coated cutting tools for micromachining applications," *Proceedings of IMechE Part L: Journal of Materials: Design and Applications,* vol. 217, no. 1, 2003, pp. 77-83.

[6] E. H. Wilson, D. F. Lawrence, K. Sridharan, and P. W. Sandstrom, "Plasma source ion implantation technology for engineering surfaces of materials," in *Proceedings of the Application of Accelerators in Research and Industry. Sixteenth International Conference, 1-5 Nov. 2000 Conference*, 2001, pp. 1032-1035.

[7] M. C. A. Nono, E. J. Corat, M. Ueda, C. Stellati, J. J. Barroso, J. R. Conrad, M. Shamim, P. Fetherston, and K. Sridharan, "Surface modification on 304 SS by plasma-immersed ion implantation to improve the adherence of a CVD diamond film," *Surface and Coatings Technology,* vol. 112, no. Compendex, 1999, pp. 295-298.

[8] A. V. Sumant, P. U. P. A. Gilbert, D. S. Grierson, A. R. Konicek, M. Abrecht, J. E. Butler, T. Feygelson, S. S. Rotter, and R. W. Carpick, "Surface composition, bonding, and morphology in the nucleation and growth of ultra-thin, high quality nanocrystalline diamond films," *Diamond and Related Materials,* vol. 16, no. 4-7, 2007, pp. 718-724.

[9] P. J. Burnett, and T. F. Page, "Investigation of Ion Implantation-Induced Near-Surface Stresses and their Effects in Sapphire and Glass," *Journal of Materials Science,* vol. 20, no. Compendex, 1985, pp. 4624-4646.

[10] K. C. Walter, M. Nastasi, N. P. Baker, C. P. Munson, W. K. Scarborough, J. T. Scheuer, B. P. Wood, J. R. Conrad, K. Sridharan, S. Malik, and R. A. Bruen, "Advances in PSII techniques for surface modification," *Surface and Coatings Technology,* vol. 103-104, no. 1, 1998, pp. 205-211.

[11] P. J. Heaney, A. V. Sumant, C. D. Torres, R. W. Carpick, and F. E. Pfefferkorn, "Diamond coatings for micro end mills: Enabling the dry machining of aluminum at the micro-scale," *Diamond and Related Materials,* vol. 17, no. 3, 2008, pp. 223-233.

[12] D. S. Knight, and W. B. White, "Characterization of diamond films by Raman spectroscopy," *Journal of Materials Research,* vol. 4, no. 2, 1989, pp. 385-393.

[13] L. Fayette, B. Marcus, M. Mermoux, G. Tourillon, K. Laffon, P. Parent, and F. Le Normand, "Local order in CVD diamond films : Comparative Raman, X-ray-diffraction, and X-ray-absorption near-edge studies," *Physical Review B (Condensed Matter),* vol. 57, no. 22, 1998, pp. 14123-14132.

[14] J. Birrell, J. E. Gerbi, O. Auciello, J. M. Gibson, D. M. Gruen, and J. A. Carlisle, "Bonding structure in nitrogen doped ultrananocrystalline diamond," *Journal of Applied Physics,* vol. 93, no. 9, 2003, pp. 5606-5612.